Chemical Geology 432 (2016) 41–53

Contents lists available at ScienceDirect

Chemical Geology

journal homepage: www.elsevier.com/locate/chemgeo

Geochemistry of fluid discharges from Peteroa volcano (Argentina-Chile) in 2010–2015: Insights into compositional changes related to the fluid source region(s)

F. Tassi [a,b,*], F. Aguilera [c], O. Benavente [d,e], A. Paonita [f], G. Chiodini [g], S. Caliro [g], M. Agusto [h], F. Gutierrez [d,e,i], B. Capaccioni [j], O. Vaselli [a,b], A. Caselli [k], O. Saltori [d,e]

[a] Department of Earth Sciences, University of Florence, Via La Pira, 4, 50121 Florence, Italy
[b] Institute of Geosciences and Earth Resources of the National Research Council (CNR-IGG), Via La Pira, 4, 50121 Florence, Italy
[c] Servicio Nacional de Geología y Minería, Avenida Santa María 0104, Santiago, Chile
[d] Centro de Excelencia en Geotermia (CEGA), Universidad de Chile, Plaza Ercilla 803, Santiago, Chile
[e] Departamento de Geología, Universidad de Chile, Plaza Ercilla 803, Santiago, Chile
[f] Istituto Nazionale di Geofisica e Vulcanologia, Via U. La Malfa 153, 90146 Palermo, Italy
[g] Istituto Nazionale di Geofisica e Vulcanologia, Osservatorio Vesuviano, Via Diocleziano, Napoli, Italy
[h] GESVA, IDEAN (UBA-CONICET), Departamento de Ciencias Geológicas, Universidad de Buenos Aires, Ciudad Universitaria, Pabellón 2, 1428EHA Buenos Aires, Argentina
[i] Advanced Mining Technology Center (AMTC), Av. Tupper 2007, piso 4, Santiago, Chile
[j] Department of Earth and Geological-Environmental Sciences, Piazza Porta San Donato, 1, 40126 Bologna, Italy
[k] Universidad de Río Negro, General Roca, Argentina

ARTICLE INFO

Article history:
Received 7 January 2016
Received in revised form 8 April 2016
Accepted 8 April 2016
Available online 10 April 2016

Keywords:
Gas geochemistry
Peteroa volcano
Magmatic degassing
Andean volcanic chain
Geochemical volcano monitoring

ABSTRACT

This study presents the first geochemical data of fluid discharges collected from February 2010 to March 2015 from the Planchón–Peteroa–Azufre Volcanic Complex (PPAVC), located in the Transitional Southern Volcanic Zone (TSVZ) at the border between Argentina and Chile. During the study period, from January 2010 to July 2011, Peteroa volcano experienced phreatic to phreatomagmatic eruption possibly related to the devastating Maule earthquake occurred on February 27, 2010. The compositional dataset includes low temperature (from 43.2 to 102 °C) gas discharges from (i) the summit of Peteroa volcano and (ii) the SE flank of Azufre volcano, both marked by a significant magmatic fluid contribution, as well as bubbling gases located at the foothill of the Peteroa volcanic edifice, which showed a chemical signature typical of hydrothermal fluids. In 2012, strong compositional changes affected the Peteroa gases from the summit area: the acidic gas species, especially SO_2, increased, suggesting an input of fluids from magma degassing. Nevertheless, the R/Ra and $\delta^{13}C$–CO_2 values decreased, which would imply an enhanced contribution from a meteoric-hydrothermal source. In 2014–2015, the chemical and isotopic compositions of the 2010–2011 gases were partially restored. The anomalous decoupling between the chemical and the isotopic parameters was tentatively interpreted as produced by degassing activity from a small batch of dacitic magma that in 2012 masked the compositional signature of the magmatic fluids released from a basaltic magma that dominated the gas chemistry in 2010–2011. This explanation reliably justifies the observed geochemical data, although the mechanisms leading to the change in time of the dominating magmatic fluid source are not clear. At this regard, a geophysical survey able to provide information on the location of the two magma batches could be useful to clarify the possible relationships between the compositional changes that affected the Peteroa fluid discharges and the 2010–2011 eruptive activity.

1. Introduction

Peteroa (35.240°S, 70.570°W, 3603 m a.s.l.), a composite stratovolcano belonging to the Transitional Southern Volcanic Zone (TSVZ) at the border between Argentina and Chile (e.g., Stern et al., 1984; Hildred and Moorbath, 1988) (Fig. 1), is part of the NNE-oriented Planchón–Peteroa–Azufre Volcanic Complex (PPAVC) (Tormey et al., 1995; Naranjo et al., 1999). The Peteroa summit is characterized by an ~5 km wide caldera, partially covered by glaciers. It consists of four craters hosting acidic lakes and one scoria cinder cone (Fig. 2) (Tormey, 2010). The last eruptive episode of Peteroa lasted from January 2010 up to July 2011 and was characterized by phreatic and phreatomagmatic eruptions with a VEI ≤2 (Haller and Risso, 2011; Aguilera et al., 2012; Naranjo, 2012). It is worth noting that the

* Corresponding author at: Department of Earth Sciences, University of Florence, Via La Pira, 4, 50121 Florence, Italy.
E-mail address: franco.tassi@unifi.it (F. Tassi).

http://dx.doi.org/10.1016/j.chemgeo.2016.04.007
0009-2541/

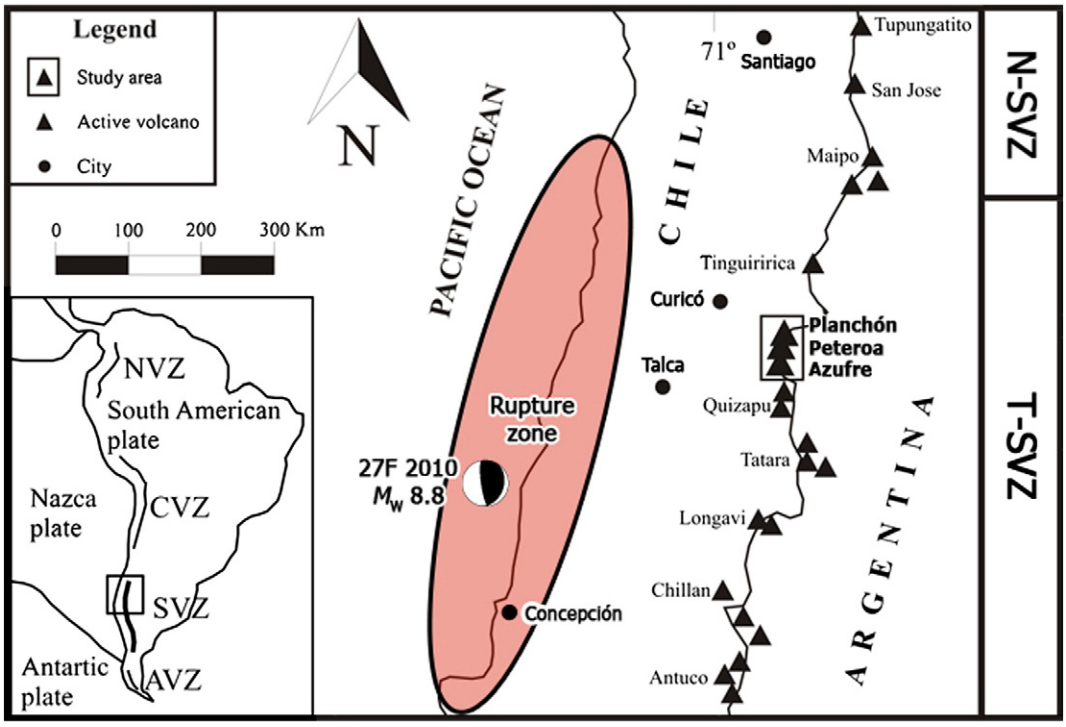

Fig. 1. Schematic map of the Northern and Transitional Southern Andean Volcanic Zone (N- and T-SVZ, respectively) and location of the Planchón–Peteroa–Azufre Volcanic Complex (PPAVC). Light red ellipse shows the approximate Maule earthquake rupture zone (Pritchard et al., 2013).

devastating February 27, 2010 Maule earthquake (M_W 8.8) that affected central-southern Chile (Jara-Muñoz et al., 2015 and references therein) was concomitant with the Peteroa volcanic activity. After this seismic event up to 2011, PPAVC suffered several M_W <3 seismic events (up to 15 km depth) (SERNAGEOMIN-OVDAS, 2010a,b,c, 2011a,b), probably related to the co-seismic release of fluids from a hydrothermal reservoir (Pritchard et al., 2013). The latter likely caused the emission of volcanic plumes from craters #2 and #3 (Fig. 2) during the last eruptive episode (Aguilera et al., 2012; Naranjo, 2012).

In this study, we present the chemical and isotopic ($\delta^{18}O$–H_2O, δD–H_2O, $\delta^{13}C$–CO_2, $^3He/^4He$, $^{40}Ar/^{36}Ar$ and $\delta^{15}N$–N_2) compositions of gases sampled during the five sampling campaigns (February 2010, March 2011, March 2012, March 2014 and March 2015) from the i) fluid discharges located at the Peteroa summit and along the SE flanks of the Azufre volcano and ii) thermal bubbling pools situated at the base of the E and SE flanks of PPAVC (Fig. 2). Chemical data of water samples collected from the lakes hosted within craters #1, #2 and #4 (Fig. 2) were also reported. The main aim was to investigate the fluid source regions and the physical–chemical processes controlling the chemistry of the Peteroa gases in 2010–2015, highlighting the temporal compositional variations and their possible relationship with the 2010–2011 eruptive activity. To the best of our knowledge, this is the first geochemical survey carried out on fluids discharged from this volcano.

2. Geological and volcanological setting

The Pleistocene–Holocene PPAVC lies on Upper Jurassic to Cretaceous continental and marine sediments (limestone, conglomerates, sandstones and gypsum sequences), pyroclastic rocks, and basaltic to rhyolitic lava flows which are locally intruded by Middle Tertiary dioritic to granodioritic plutons (Tormey et al., 1989, 1995; Naranjo et al., 1999; Naranjo and Haller, 2002). These rock formations are variably folded and thrusted, given the occurrence of NNE-oriented reverse faults pertaining to the Malargüe fold-and-thrust belt (Giambiagi et al., 2003).

The spatial orientation of PPAVC, as well as the location of the thermal manifestations (e.g., hot springs, bubbling pools, mud pools, fumaroles, steaming grounds) recognized N, E and SE of the volcanic complex, is controlled by the occurrence of these reverse faults (Cembrano and Lara, 2009; Gutierrez et al., 2012). At a regional scale, the volcanic activity in the TSVZ area is related to the subduction of the Nazca beneath the South American plates (Barazangi and Isacks, 1976; Cande and Leslie, 1986, 1987). Azufre volcano is the oldest (<1.20 My) and largest (~69 km^3) edifice of PPAVC, consisting of basaltic andesite lava and pyroclastic flows, dacitic lava flows and domes, and lahars deposits. Planchón volcano (6 km north of the Azufre cone) was built in 3 different phases: i) Planchón I (from ~14 to ~12 ky), with basaltic and basaltic andesite lava flows, pyroclastic deposits and minor lahars deposits having a total volume of ~43 km^3; ii) Planchón–Teno (~12 ky), an ~10 km^3 debris avalanche deposit produced by the collapse of the western flank of Planchón I (Hauser 1990, 1993); iii) Planchón II (from ~12 to ~7 ky), consisting of basaltic to basaltic andesitic lava flows and pyroclastic sequences, and lahars deposits whose total volume is ~5 km^3. Peteroa volcano is the smallest (<1 km^3) and youngest (<7 ky) edifice. Its activity is characterized by basaltic andesite to andesitic lava flows and basaltic andesite to dacitic pyroclastic flows, surge and fall deposits. According to Tormey et al. (1995), the volcanic products of PPAVC evolved from basalts and, secondarily, dacites (Azufre–Planchón) sourced from relatively moderate-pressure (4 to 8 kbar), to andesite (Peteroa), produced by magma mixing processes at relatively shallow depth. NNE-oriented reverse faults, developed in a compressive regime caused by the Malargüe fold and thrust belt (Ramos et al. 2004), controlled the spatial orientation of PPAVC (Cembrano and Lara, 2009), as well as the location of the thermal manifestations (e.g., hot springs, bubbling pools, mud pools, fumaroles, steaming grounds) recognized at N, E and SE of the volcanic complex (Gutierrez et al., 2012).

Fifteen glaciers, whose size significantly reduced in the last years and currently occupying a surface of ~20 km^2, occur at the PPAVC summit and its surroundings (Liaudat et al., 2014).

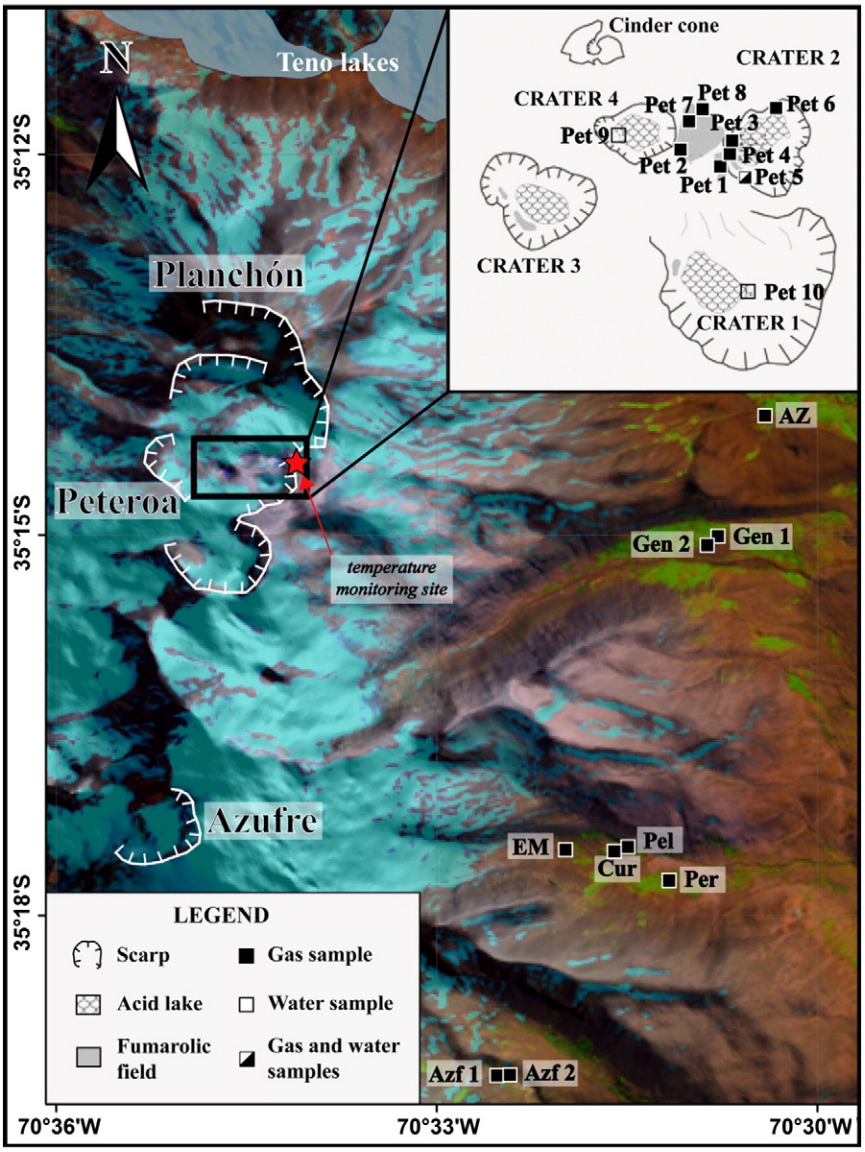

Fig. 2. Satellite image of the Planchón–Peteroa–Azufre Volcanic Complex (PPAVC). Crater zone at Peteroa volcano, fumarolic fields, crater lakes, thermal springs and location of the sampling sites are shown. Filled squares: gas sample; half-filled square: gas and water sample; open square: water sample. Red star corresponds to the soil and air temperature monitoring site of Liaudat et al. (2014).

3. Historical eruptive activity

Peteroa is the only volcano of PPAVC that has experienced historical eruptive activity, during which phreatic and phreatomagmatic events (VEI ≤3) occurred (1660, November–December 1751, March 1762, 1835, February 1837, 1842, 1860, 1869, 1872, 1878, 1889–1894, 1938, November 1959, August 1960, January 1962, February 1967, February 1991 and November 1998) (Gonzalez-Ferrán, 1995; Naranjo et al., 1999; Naranjo and Haller, 2002). The last eruptive activity from crater #3 (Fig. 2), from January 2010 to July 2011, consisted of four stages, as follows:

Stage 1 (from 4th January to 8th August 2010): Emission of a 100–200 m high white (gas and vapor) plume possibly related to the occurrence of phreatic explosions in the SW side of crater #3.
Stage 2 (from 4th September to 1st November 2010): Emission of a plume having a maximum height of ~3 km that was visible up to 345 km toward ESE. Ash fall deposits covered an area of 1265 km^2. Non-vesiculated juvenile fragments were characterized by SiO_2 contents ranging from 55 to 57.5 wt.% (Haller and Risso, 2011), similar to those of the volcanic products emitted during the 1837 eruption (Naranjo, 2012).
Stage 3 (from 17th February to 20th May 2011): Emission of a white ESE-oriented plume (up to ~1000 m above the crater rim). Tephra deposits consist of poorly vesicular andesitic fragments of lava, glassy lava, quartz, plagioclase and pyroxene crystals with no evidence of hydrothermal alteration (Aguilera et al., 2012).
Stage 4 (from 17th June to 13th July 2011): Sporadic explosions produced a 500–2000 m high, SE-oriented intermittent plume.

The epicenters of the seismic activity recorded during the 2010–2011 eruptive activity were located in two main zones, 16–33 km NE and 5–7 km N from active crater, with focus located at 1–30 km and 1–8 km depth, respectively (SERNAGEOMIN-OVDAS, 2010a,b,c, 2011a, b). A third epicenter zone, 9–20 km SE from the active craters and with focus at 1–15 km depth, was recognized. Most earthquakes

(>85%) were interpreted as produced by rock fracturing, whereas few of them were related to underground fluid circulation (SERNAGEOMIN-OVDAS, 2010a,b,c, 2011a,b).

4. Material and methods

4.1. Gas and water sampling

Gas samples were collected from different zones (Fig. 2), as follows: (1) between craters #2 and #3 (Pet1, Pet2, Pet7 and Pet8); (2) the bottom of crater #2 (Pet3, Pet4, Pet5 and Pet6); (3) the SE flank of the Azufre volcano (Azf1 and Azf2); (4) the Valenzuela valley (AZ); (5) the Glacial valley (Gen1 and Gen2); (6) the Los Azufres valley (EM, Cur, Pel and Per). Gases from the fluid emissions were conveyed into glass flasks using a 1 m long titanium tube (Ø = 2.5 cm) that was inserted into the gas vent and connected through glass-dewared tubes to the sampling flasks. A plastic funnel upside-down submerged in the pools and connected to the sampling flasks through tygon tubes was used to sample the bubbling gases. Sampling flasks used to collect gases from both the discharges of the volcano summit and the bubbling pools consisted of pre-evacuated 60-mL glass thorion-tapped flask filled with 20 mL of 4 N NaOH and 0.15 M $Cd(OH)_2$ suspension (Montegrossi et al., 2001). During sampling, water vapor and acidic gas species (CO_2, SO_2, HCl and HF) dissolved in the alkaline solution, whereas H_2S formed insoluble CdS. Low-solubility gas species (N_2, O_2, CO, H_2, He, Ar, Ne, CH_4 and light hydrocarbons) were concentrated in the sampling flask headspace. Aliquots of vapor condensates (for the analysis of $\delta^{18}O$ and δD in water vapor) and dry gases (for the analysis of CO and $^{13}C/^{12}C$ ratio in CO_2) were sampled using an ice-cooled glass tube connected to the gas sampling line (Montegrossi et al., 2001; Vaselli et al., 2006). In 2012, six gas samples were collected in 100 mL sampling flasks filled with 50 mL of 4 N NaOH for the analysis of $\delta^{15}N$.

In 2011, three water samples from the crater lakes hosted in craters #1 (Pet10), #2 (Pet5) and #4 (Pet9) (Fig. 2) were collected in 200 mL sterile polyethylene bottles, after filtering at 0.45 μm. Not filtered water was collected in 100 mL dark glass bottles for the analysis of $\delta^{18}O$ and δD. Using this sampling method, one water sample from the lake hosted in crater #2 (Pet5) was also collected in 2012. In 2011 and 2012, water aliquots from the pools where the bubbling gases were collected (Pel, Gen2 and Cur) were also sampled for the analysis of $\delta^{18}O$ and δD.

4.2. Chemical and isotopic (R/Ra, $\delta^{13}C$–CO_2, $^{40}Ar/^{36}Ar$ and $\delta^{15}N$) analysis of gases and steam ($\delta^{18}O$ and δD)

Inorganic gases (N_2, Ar + O_2, H_2, He and CO) in the flask headspace of samples collected in 2010, 2011, 2014 and 2015 were analyzed at the Department of Earth Sciences of the University of Florence (Italy) using a Shimadzu 15A gas chromatograph (GC) equipped with a 10 m long 5A molecular sieve column and a thermal conductivity detector (TCD). Argon and O_2 were analyzed using a Thermo Focus gas chromatograph equipped with a 30 m long capillary molecular sieve column and a TCD. A Shimadzu 14A gas chromatograph (GC) equipped with a 10-m-long stainless steel column packed with Chromosorb PAW 80/100 mesh coated with 23% SP 1700 and a flame ionization detector (FID) was used to analyze CH_4 and light hydrocarbons. The liquid and the solid precipitate in the alkaline suspension were separated by centrifugation at 4000 rpm for 30 min. The liquid phase was used to analyze 1) CO_2, as CO_3^{2-}, by automatic titration (AT; Metrohm Basic Titrino) with a 0.5 N HCl solution; 2) HCl, as Cl^-, by ion chromatography (IC; Metrohm 761); 3) SO_2, as SO_4^{2-}, after oxidation with 5 mL H_2O_2 (33%) by IC. Using 5 mL H_2O_2 (33%), CdS in the solid precipitate was oxidized to SO_4^{2-} that was analyzed by IC for determining H_2S concentrations (Montegrossi et al., 2001). HF concentrations were calculated on the basis of F^- concentrations in the condensates. The analytical errors for AT, GC and IC analyses were <5%.

The analysis of $^{13}C/^{12}C$ of CO_2 ($\delta^{13}C$–CO_2, expressed as ‰ vs. V-PDB) of the 2010, 2011, 2014 and 2015 samples were carried out with a Finningan Delta S mass spectrometer after standard extraction and purification procedures of the gas mixtures (Evans et al., 1998; Vaselli et al., 2006). Standards used for estimation of external precision were Carrara and San Vincenzo marbles (Internal), NBS18 and NBS19 (International), whereas the analytical error and the reproducibility were ±0.05‰ and ±0.1‰, respectively. The $\delta^{13}C$–CO_2 values of the 2012 samples were carried out following chromatographic separation using GBII. The analytical error was ±0.06‰.

The He isotopic ratios (expressed as R/Ra, where R is the $^3He/^4He$ measured ratio and Ra is the $^3He/^4He$ ratio in the air: 1.39×10^{-6}; Mamyrin and Tolstikhin, 1984) were determined at the INGV laboratories of Palermo (Italy) on gas aliquots transferred from the flask headspace into pre-evacuated 50 mL flasks. After standard purification procedures, Ne was cryogenically separated from Heat 77 K by absorption in a charcoal trap cooled at 12 K. The abundances and isotope compositions of He, as well as the $^4He/^{20}Ne$ ratios, were then determined by separately admitting He and Ne into a split flight tube mass spectrometer (Helix SFT). The analytical error was ≤0.3% (Paonita et al., 2013). The measured R/Ra values were corrected for atmospheric contamination using the $^4He/^{20}Ne$ ratios (Poreda and Craig, 1989), as follows:

$$Rc/Ra = [(R/Ra_{meas}) - r)]/(1 - r) \quad (1)$$

where r is $(^4He/^{20}Ne)_{air}/(^4He/^{20}Ne)_{measured}$ [$(^4He/^{20}Ne)_{air} = 0.318$; Ozima and Posodek, 1983)].

The chemical composition and the $\delta^{15}N$ (expressed as ‰ vs. air) and $^{40}Ar/^{36}Ar$ ratios in the 2012 gas samples were determined at the INGV laboratories of Naples (Italy) using an Agilent 6890N gas chromatograph (GC) coupled with a Finnigan Delta plusXP continuous-flow mass spectrometer (MS). The GC was equipped with a molecular sieve column (MS 5 Å capillary, 30 m × 0.53 mm × 50 μm; He carrier gas), TCD detector and a post column switching device (Denswitch) that had the following function: i) to split the column gas flow to the TCD detector and to the MS, and ii) to invert the column flow after the species of interest (Ar and N_2) had reached the detector, preventing undesirable species (mainly CO and water) from reaching the MS. To allow simultaneous determination of ^{36}Ar and ^{15}N, the MS was equipped with a standard triple collector. Initially, the ion beam was focused to send mass 36 to the more sensitive cup. After recording the mass 36 peak, the magnetic field was switched to focus the ion beams of masses 28, 29 and 30 on the three cups using a jump calibration procedure taking into account any hysteresis of the magnet. Analytical errors were: $\delta^{15}N$ ± 0.1‰, ^{36}Ar < 1%, ^{40}Ar < 3%.

The $^{18}O/^{16}O$ and $^2H/^1H$ isotopic ratios ($\delta^{18}O$–H_2O and δD–H_2O, expressed as ‰ vs. V-SMOW) of the condensates and water samples were determined using a Finnigan Delta Plus XL mass spectrometer at the Geokarst Engineering Laboratory (Trieste, Italy). Oxygen isotopes were analyzed following the method described by Epstein and Mayeda (1953). Hydrogen isotopes were analyzed on H_2 generated by the reaction of 10 μL water with metallic zinc at 500 °C, according to the analytical procedure described by Coleman et al. (1982). The analytical errors were ±0.1‰ for $\delta^{18}O$ and ±0.1‰ for δD, using V-SMOW and SLAP as analytical standards and AR-1 as an internal standard. The $\delta^{18}O$–H_2O and δD–H_2O values of the 2012 gas samples were analyzed at the INGV laboratories of Naples (Italy) using a Finnigan Delta plusXP continuous-flow mass spectrometer (MS) coupled with a GasbenchII gas-chromatographic device (GBII), using equilibration techniques with CO_2 for oxygen (Epstein and Mayeda, 1953), and with H_2 for hydrogen (Nelson 2000). The analytical errors were ±0.08‰ and ±1‰ for δD and $\delta^{18}O$, respectively.

Table 1
Type, date, geographical coordinates (UTM, WGS 85 Zone 19), altitude (m a.s.l.), outlet temperatures (in °C), chemical composition (dry gas fraction) of inorganic gases and CH_4 (in mmol/mol), and total concentration of the dry gas fraction (Xg in %) for the PPAVC gas discharges.

ID	type	date	latitude	longitude	altitude	T	CO_2	HCl	HF	SO_2	H_2S	N_2	CH_4	Ar	O_2	H_2	He	CO	Xgas %
Pet1	Fumarole	February 2010	6099208	357027	3436	91.8	978	0.25	0.011	0.12	19	1.6	0.24	0.026	0.056	0.36	0.0032	0.0026	9.5
Pet2	Fumarole	February 2010	6099171	356908	3434	102	961	0.19	0.021	0.17	35	2.7	0.29	0.024	0.049	0.38	0.0028	0.0031	8.9
Pet1	Fumarole	March 2011	6099208	357027	3436	87.7	975	0.37	0.010	0.55	21	2.6	0.13	0.0043	0.0065	0.25	0.0014	0.015	14.6
Pet3	Fumarole	March 2011	6099212	357037	3374	88.4	979	0.38	0.012	0.51	18	2.3	0.098	0.0016	0.0047	0.21	0.0012	0.0092	12.1
Pet4	Fumarole	March 2011	6099169	357042	3401	88.4	978	0.32	0.012	0.40	18	2.5	0.11	0.0042	0.028	0.18	0.0013	0.0089	14.7
Pet5	Fumarole	March 2011	6099157	357050	3331	43.2	986	0.24	0.008	0.31	11	2.5	0.12	0.0076	0.028	0.13	0.0015	0.0050	21.8
Pet6	Fumarole	March 2011	6099288	357171	3358	87.9	978	0.31	0.010	0.41	19	2.4	0.10	0.0047	0.0068	0.23	0.0015	0.015	15.0
Pet7	Fumarole	March 2011	6099257	356939	3411	88.3	980	0.38	0.011	0.54	16	2.3	0.091	0.0043	0.0010	0.28	0.0022	0.012	15.4
Pet1	Fumarole	March 2012	6099208	357027	3436	87.8	382	14	1.3	448	145	9.5	0.014	0.025	0.0004	0.32	0.0037	0.0012	3.4
Pet3	Fumarole	March 2012	6099212	357037	3374	89.4	380	13	1.3	450	148	7.3	0.012	0.0079	0.0009	0.23	0.0034	0.0010	2.8
Pet7	Fumarole	March 2012	6099257	356939	3411	87.9	370	13	1.2	456	153	6.5	0.013	0.0047	0.0005	0.36	0.0036	0.0009	3.8
Pet8	Fumarole	March 2012	6099317	356996	3446	87.9	282	12	1.2	534	162	7.8	0.015	0.014	0.0007	0.47	0.0043	0.0008	3.0
Azf1	Fumarole	March 2012	6090273	359938	2758	88.7	794	5.3	0.8	38	156	3.2	0.086	0.046	0.011	2.6	0.0011	0.0069	3.11
Azf2	Fumarole	March 2012	6090246	359912	2766	87.8	781	4.7	0.9	26	181	3.6	0.094	0.041	0.0060	3.1	0.0009	0.0087	2.56
Pet7	Fumarole	March 2014	6099212	357037	3374	89.5	916	0.56	0.035	31	47	5.3	0.089	0.007	0.0011	0.41	0.0033	0.0026	5.8
Pet1	Fumarole	April 2015	6099208	357027	3436	88.1	958	0.31	0.016	1.2	35	4.9	0.16	0.0045	0.0039	0.32	0.0018	0.0074	11.3
Pet7	Fumarole	April 2015	6099212	357037	3374	89.3	955	0.22	0.017	1.6	39	4.2	0.11	0.0053	0.0025	0.25	0.0017	0.0066	10.4
Gen1	Bubbling pool	February 2010	6098170	362325	2472	26.3	990	<0.01	<0.005	<0.01	<0.01	8.1	1.4	0.15	0.55	0.0048	0.0078	<0.0005	98.5
Gen2	Bubbling pool	February 2010	6098014	362203	2476	28.2	993	<0.01	<0.005	<0.01	<0.01	5.3	1.3	0.12	0.62	0.0061	0.0052	<0.0005	98.7
AZ	Bubbling pool	February 2010	6099896	36287	2435	24.1	994	<0.01	<0.005	<0.01	<0.01	3.8	1.4	0.098	0.49	0.0044	0.0044	<0.0005	99.1
EM	Bubbling pool	February 2010	6093572	361212	2507	38.3	996	<0.01	<0.005	<0.01	<0.01	2.7	1.0	0.095	0.36	0.0056	0.0056	<0.0005	97.2
Per	Bubbling pool	February 2010	6093131	361819	2472	37.4	994	<0.01	<0.005	<0.01	<0.01	3.9	1.4	0.13	0.64	0.0049	0.0031	<0.0005	97.2
Pel	Bubbling pool	February 2010	6093577	361327	2490	43.7	992	<0.01	<0.005	<0.01	<0.01	6.5	1.6	0.048	0.12	0.0038	0.0061	<0.0005	96.5
Pel	Bubbling pool	March 2011	6093577	361327	2490	46.2	996	<0.01	<0.005	<0.01	<0.01	1.8	1.4	0.039	0.54	0.0056	0.0026	<0.0005	97.7
Gen2	Bubbling pool	March 2012	6098014	362203	2476	28.2	993	<0.01	<0.005	<0.01	<0.01	5.3	1.1	0.13	0.62	0.0061	0.0052	<0.0005	93.5
Cur	Bubbling pool	March 2012	6098014	362203	2476	39.0	991	<0.01	<0.005	<0.01	<0.01	6.2	1.8	0.15	0.96	0.0044	0.0040	<0.0005	91.6
Gen2	Bubbling pool	March 2015	6098014	362203	2476	24.1	992	<0.01	<0.005	<0.01	<0.01	5.6	1.3	0.14	0.55	0.0035	0.0031	<0.0005	94.1
Pel	Bubbling pool	March 2015	6093577	361327	2490	42.3	992	<0.01	<0.005	<0.01	<0.01	6.2	1.5	0.068	0.69	0.0046	0.0043	<0.0005	95.8
AZ	Bubbling pool	March 2015	6099896	36287	2435	38.7	994	<0.01	<0.005	<0.01	<0.01	4.5	1.2	0.11	0.36	0.0041	0.0039	<0.0005	98.9

4.3. Chemical analysis of waters

Temperature and pH of lake water were determined in the field. Water samples were analyzed for major cations (Na^+, K^+, Ca^{2+}, Mg^{2+}, and NH_4^+) and anions (F^-, Cl^- SO_4^{2-}, Br^- and NO_3^-) by IC (Metrohm 861 and Metrohm 761, respectively). The analytical error was ≤5%.

5. Results

5.1. Chemical composition of gases

Location of the sampling points (UTM coordinates; WGS 84 Zone 19), altitude (m a.s.l.), outlet temperatures of the gas vents, water temperatures of the bubbling pools (°C) and chemical composition (expressed in mmol/mol) of the dry gas fraction (Xg in %) are reported in Table 1.

The gas discharges from the summit area, consisting of fumarolic-like vents whose outlet temperature ranged from 43.2 to 102 °C, were dominated by water vapor (Xg from 2.8% to 21.8%). The dry gas composition of samples collected in 2010, 2011 and 2015 from the Peteroa summit was dominated by CO_2 (up to 986 mmol/mol), followed by H_2S (up to 39 mmol/mol). Sulfur dioxide, HCl and HF concentrations were relatively low (up to 1.6, 0.38 and 0.021 mmol/mol, respectively). Nitrogen and H_2 concentrations were in a narrow range, from 1.6 to 4.9, and from 0.13 to 0.38 mmol/mol, respectively, whereas those of CH_4, O_2, Ar, He, and CO were up to 0.29, 0.056, 0.026, 0.0032, and 0.015 mmol/mol, respectively (Table 1). Light hydrocarbons (C_2–C_7) mainly consisted of alkanes, whose sum was up to 0.0118 mmol/mol, with significant concentrations of alkenes and aromatics, dominated by i-C_4H_8 (up to 0.0032 mmol/mol) and C_6H_6 (0.0025 mmol/mol), respectively. Thiophene (C_4H_4S) and furane (C_4H_4O) were also detected at concentrations up to 0.00073 and 0.000021 mmol/mol, respectively (Table 2).

The composition of the Peteroa gases collected in March 2012 was strongly different with respect to those previously sampled. The main compositional differences can be summarized, as follows:

SO_2 concentration (up to 534 mmol/mol) was three orders of magnitude higher whereas those of CO_2 ranged from 282 to 382 mmol/mol. Similar changes were also shown by the concentrations of other acidic species, i.e. H_2S, HCl and HF (up to 162, 14 and 1.3 mmol/mol, respectively), whereas N_2 and H_2 showed slight increases (from 6.5 and 9.5 and from 0.23 to 0.47 mmol/mol, respectively). On the contrary, CH_4 and CO significantly decreased, down to ≤0.015 and ≤0.0012 mmol/mol, respectively. Hydrocarbon concentrations decreased, especially the C_4-compounds and C_7H_8 that were below the detection limit (0.0000005 mmol/mol).

In 2014, the Peteroa fluid discharges showed compositional features similar to those recorded for the 2010–2011 and 2015 samples, with the exception of SO_2, H_2S and N_2 that were characterized by slightly higher concentrations (up to 1.6, 39 and 4.9 mmol/mol, respectively).

The composition of the fumaroles from the flanks of Azufre volcano (March 2012) partially resembles that of the gases collected from the Peteroa summit in the same period, although the former had significantly higher CO_2 and H_2 concentrations (up to 794 and 3.1 mmol/mol, respectively) and lower SO_2 (up to 38 mmol/mol).

Gases collected from the bubbling pools in 2010, 2011, 2012 and 2015, whose temperatures ranged from 24 to 46.2 °C, were characterized by a CO_2-dominated (up to 996 mmol/mol) chemical composition, absence of acidic gases and CO, significant concentrations of N_2 and CH_4 (up to 8.1 and 1.8 mmol/mol, respectively), and relatively low concentrations of H_2 (≤0.0078 mmol/mol). Light hydrocarbons mostly consisted of C_2H_6 (up to 0.027 mmol/mol), with minor C_3–C_4 alkanes (sum up to 0.0035 mmol/mol), C_6H_6 (up to 0.0066 mmol/mol) and C_3H_6 (up to 0.00016 mmol/mol), whereas C_2H_4, C_4H_4S and C_4H_4O were not detected (Table 2). The composition of bubbling gases (Gen2, AZ and Pel) did not show significant temporal changes.

5.2. Isotopic composition of gases (Rc/Ra, $\delta^{13}C$–CO_2, $^{40}Ar/^{36}Ar$, $\delta^{15}N$–N_2) and steam ($\delta^{18}O$–H_2O and δD–H_2O)

The isotopic compositions of water vapor ($\delta^{18}O$–H_2O and δD–H_2O), CO_2 ($\delta^{13}C$–CO_2), He (Rc/Ra), Ar ($^{40}Ar/^{36}Ar$), and N_2 ($\delta^{15}N$–N_2) in the Peteroa gas samples are reported in Table 3. The $\delta^{18}O$–H_2O and δD–

Table 2
Concentrations of C_2–C_7 hydrocarbons (in mmol/mol) for the PPAVC gas discharges.

ID	C_2H_6	C_2H_4	C_3H_8	C_3H_6	i-C_4H_{10}	n-C_4H_{10}	i-C_4H_8	C_4H_4O	C_6H_6	C_4H_4S	C_7H_8
Pet1	0.0037	0.000012	0.00027	0.000042	<0.0000005	0.00011	0.0026	0.000021	0.0018	0.00069	0.00011
Pet2	0.0042	0.000022	0.00071	0.000070	<0.0000005	0.00012	0.0032	0.000019	0.0021	0.00073	0.00012
Pet1	0.0054	0.000016	0.00087	0.000087	<0.0000005	0.00011	0.0018	0.000013	0.0025	0.00039	0.000053
Pet3	0.0048	0.000011	0.00057	0.000055	<0.0000005	0.00019	0.0027	0.000016	0.0020	0.00041	0.000047
Pet4	0.0048	0.000018	0.00069	0.000073	<0.0000005	0.00016	0.0023	0.000014	0.0023	0.00042	0.000078
Pet5	0.0052	0.000011	0.00078	0.000088	<0.0000005	0.00018	0.0022	0.000014	0.0023	0.00037	0.000050
Pet6	0.0064	0.000017	0.00075	0.000054	<0.0000005	0.00012	0.0019	0.000011	0.0022	0.00033	0.000075
Pet7	0.0047	0.000013	0.00077	0.000060	<0.0000005	0.00015	0.0020	0.000010	0.0022	0.00038	0.000050
Pet1	0.00020	0.0000009	0.000018	0.0000020	<0.0000005	<0.0000005	<0.0000005	0.00083	0.000012	<0.0000005	<0.0000005
Pet3	0.00022	0.0000008	0.000020	0.0000014	<0.0000005	<0.0000005	<0.0000005	0.00059	0.000035	<0.0000005	<0.0000005
Pet7	0.00022	0.0000012	0.000021	0.0000019	<0.0000005	<0.0000005	<0.0000005	0.00065	0.000032	<0.0000005	<0.0000005
Pet8	0.00028	0.0000012	0.000024	0.0000024	<0.0000005	<0.0000005	<0.0000005	0.00045	0.000012	<0.0000005	<0.0000005
Azf1	0.00039	0.0000008	0.000032	0.0000016	<0.0000005	<0.0000005	<0.0000005	0.00011	0.000088	<0.0000005	<0.0000005
Azf2	0.00041	0.0000007	0.000033	0.0000019	<0.0000005	<0.0000005	<0.0000005	0.000080	0.000071	<0.0000005	<0.0000005
Pet7	0.00061	0.0000007	0.000051	0.0000039	<0.0000005	<0.0000005	<0.0000005	0.00011	0.000091	<0.0000005	<0.0000005
Pet1	0.0044	0.000012	0.00069	0.000071	<0.0000005	<0.0000005	0.00015	0.000011	0.0015	0.00039	0.000055
Pet7	0.0039	0.000013	0.00055	0.000066	<0.0000005	<0.0000005	0.00021	0.000015	0.0018	0.00045	0.000071
Gen1	0.027	<0.0000005	0.0012	0.00013	0.00019	0.000056	0.000034	<0.0000005	0.00069	<0.0000005	0.000026
Gen2	0.017	<0.0000005	0.00080	0.00013	0.00014	0.000045	0.000048	<0.0000005	0.00059	<0.0000005	0.000023
AZ	0.017	<0.0000005	0.00091	0.00012	0.00015	0.000061	0.000026	<0.0000005	0.00068	<0.0000005	0.000027
EM	0.023	<0.0000005	0.00086	0.00010	0.00016	0.000075	0.000060	<0.0000005	0.00090	<0.0000005	0.000042
Per	0.024	<0.0000005	0.0011	0.00012	0.00018	0.000079	0.000048	<0.0000005	0.00076	<0.0000005	0.000036
Pel	0.019	<0.0000005	0.00091	0.000098	0.00016	0.000068	0.000026	<0.0000005	0.00075	<0.0000005	0.000021
Pel	0.0043	<0.0000005	0.00038	0.000031	0.000024	0.000013	<0.0000005	<0.0000005	0.000003	<0.0000005	<0.000001
Gen2	0.017	<0.0000005	0.0019	0.000057	0.00044	0.00012	0.000071	<0.0000005	0.0056	<0.0000005	0.000061
Cur	0.024	<0.0000005	0.0018	0.000062	0.00053	0.00014	0.000088	<0.0000005	0.0066	<0.0000005	0.000093
Gen2	0.019	<0.0000005	0.0026	0.000036	0.00033	0.00016	0.000065	<0.0000005	0.0061	<0.0000005	0.000055
Pel	0.026	<0.0000005	0.0033	0.000074	0.00012	0.000045	0.000021	<0.0000005	0.00088	<0.0000005	0.000015
AZ	0.022	<0.0000005	0.0031	0.00016	0.00011	0.00011	0.000033	<0.0000005	0.00055	<0.0000005	0.000013

Table 3
Isotopic composition of steam ($\delta^{18}O$ and δD in ‰ vs. V-SMOW), carbon in CO_2 ($\delta^{13}C$ in ‰ vs. V-PDB), He (as R/Ra, where R is the measured ratio and Ra is that of the air: 1.39×10^{-6}; Mamyrin and Tolstikhin 1984), Ar ($^{40}Ar/^{36}Ar$), and N_2 ($\delta^{15}N$ in ‰ vs. air) for the PPAVC gas discharges. The $\delta^{18}O$ and δD values of rainwater collected in this section of the Andes at 4,000 m a.s.l. are also reported. The measured R/Ra values were corrected for air contamination on the basis of the $^4He/^{20}Ne$ ratios (Poreda and Craig, 1989). The Ar^* values are air-free Ar concentrations computed as follows: $Ar^* = {}^{40}Ar - ({}^{40}Ar/{}^{36}Ar)_{air} \times {}^{36}Ar$, where ^{40}Ar is from Table 2 and ^{36}Ar is assumed to be entirely from atmosphere.

ID	Date	Rc/Ra	$^{40}Ar/^{36}Ar$	He/Ne	$\delta^{13}C–CO_2$	$\delta D–H_2O$	$\delta^{18}O–H_2O$	$\delta^{15}N$	$^{40}Ar^*$	$CO_2/^3He \times 10^{10}$
Pet1	March 2011				−6.11	−80	−5.9			
Pet3	March 2011	6.87	455	711	−7.60	−73	−4.3		0.0006	8.5
Pet4	March 2011				−3.02	−74	−3.6			
Pet5	March 2011	7.11	378	289	−3.56	−74	−3.5		0.0017	6.7
Pet6	March 2011				−2.02	−80	−4.8			
Pet7	March 2011	6.59	491	511	−5.82				0.0017	4.9
Pet1	March 2012	4.43	313	305	−11.2	−115	−15.7	4.27	0.048	1.7
Pet3	March 2012	4.46	337	387	−11.2	−76	−10.5	4.79	0.028	1.8
Pet7	March 2012	4.46	367	662	−11.6	−98	−13.4	5.00	0.036	1.7
Pet8	March 2012	4.44	314	398	−11.4	−103	−15.1	4.47	0.024	1.4
Azf2	March 2012				−11.9	−101	−14.9			
Pet7	March 2014	5.62		454						3.6
Pet1	April 2015	6.68		456	−7.54	−98	−13.7			5.7
Pet7	April 2015	6.51		511	−6.15	−119	−17.2			6.2
Pel	March 2011	3.69	328	131	−13.2	−106	−14.7		0.0039	7.5
Gen2	March 2012	5.94		75	−12.6	−103	−15.1	1		2.0
Cur	March 2012	1.19	295	36	−12.6	−98	−13.4	−0.34		1.4
Gen2	March 2015	3.21		35	−12.6					6.4
Pel	March 2015	3.12		115	−12.1					5.0
rain	March 2011					−118	−15.8			

H_2O values of the fluid discharges sampled in 2010–2011 from the Peteroa summit ranged from −5.9‰ to −3.5‰ and from −80‰ to −73‰ vs. V-SMOW, respectively, whereas those of the 2012 and 2015 gases from both the Peteroa summit and the Azufre volcano were significantly more negative, down to −17.2‰ and −119‰ vs. V-SMOW, respectively, similar to those of the waters from the bubbling pools (down to −15.1‰ and −106‰ vs. V-SMOW, respectively). The Peteroa summit gases were also affected by significant temporal changes of the $\delta^{13}C–CO_2$ values, which in 2010, 2011 and 2015 ranged from −7.60‰ to −2.02‰ vs. V-PDB, whereas in 2012 were ≤−11.2‰ vs. V-PDB, similar to those of the Azufre fumarole (−11.9‰ vs. V-PDB) and the bubbling pools (−13.2‰ to −12.1‰ vs. V-PDB).

In 2012, the Rc/Ra values, which in 2010–2011 ranged from 6.87 to 7.11, strongly decreased (from 4.43 to 4.46), whereas afterwards they showed an opposite trend, progressively increasing up to 5.62 (2014) and 6.68 (2015). The bubbling gases showed a wide range of Rc/Ra values: from 1.19 to 5.94. The $^{40}Ar/^{36}Ar$ ratios in the gases from the Peteroa summit (up to 491) were significantly higher than that of air (295.5), whereas in the bubbling gases they ranged from 295 to 328. The $\delta^{15}N$ values in the 2011–2012 summit fluid discharges were in a relatively narrow range (from 4.27‰ to 5‰ vs. air), whereas in the Cur and Gen2 bubbling gases they were −0.34‰ and 1‰ vs. air, respectively.

5.3. Chemical and isotopic ($\delta^{18}O–H_2O$ and $\delta D–H_2O$) compositions of crater lakes

Temperature, pH and chemical composition of the crater lakes hosted in craters #1 (Pet10), #2 (Pet5) and #4 (Pet9) (Fig. 2) are reported in Table 4. Temperature and pH ranged from 7.4 to 43.2 °C and from 1.49 to 2.91, respectively. The lake chemistry was invariably dominated by SO_4^{2-} (up to 3300 mg/L; Pet5), whereas Cl^- concentrations ranged from 44 to 660 mg/L. The most abundant cation was Ca^{2+} (up to 520 mg/L), followed by Mg^{2+} (380 mg/L), Na^+ (180 mg/L) and K^+ (130 mg/L). Significant concentrations of minor species, such as F^-, NH_4^+, NO_3^- and Br^- (up to 39, 10, 2.0 and 1.4 mg/L, respectively), were measured. The $\delta^{18}O–H_2O$ and $\delta D–H_2O$ values ranged from −10 to −9.5‰ and from −80‰ to −74‰ vs. V-SMOW, respectively.

6. Discussion

6.1. Fluid source regions

Clues of magma degassing are clearly recognizable in the Peteroa and Azufre fluid discharges, since they were marked by the presence of SO_2 (Table 1) (Giggenbach, 1987). Moreover, the occurrence of HCl and HF at significant concentrations (Table 1), likely produced by high-temperature reactions involving chemical species (F^- and Cl^-) released from the magmatic source, was recognized. Notwithstanding the evident contribution of magmatic fluids, the outlet temperatures of the summit gases were similar to that of boiling water at 3400 m a.s.l. (~88 °C), indicating the occurrence of a shallow aquifer fed by water vapor condensation, as well as rain and glacier melting, as confirmed by the meteoric isotopic signature of the crater lakes (Fig. 3). Hence, the low pH and high SO_4^{2-} and Cl^- contents of the crater lakes (Table 4), closely resembling that of the so-called "Active" crater lakes (Varekamp et al., 2000), were likely produced by the interaction of meteoric water with acidic gases uprising from a magmatic source. The interaction between deep-originated gases and meteoric water may explain the occurrence, although at relatively low concentrations, of atmospheric gases in the fluids from the summit area. Hydrogen sulfide, CH_4, H_2, CO and light hydrocarbons likely originated at hydrothermal conditions, hence in a zone located at intermediate depth between the degassing magma and the surface. Therefore, the fluid source of Peteroa–Azufre fluid discharges basically consisted of a magmatic-hydrothermal reservoir, as commonly found in active volcanoes from convergent plate boundaries (e.g., Giggenbach, 1987, 1996).

Table 4
Temperature (in °C), pH, chemical composition (in mg/L) and isotopic composition of waters ($\delta^{18}O$ and δD in ‰ vs. V-SMOW) from lakes of the Peteroa summit craters.

ID	Crater	Date	Latitude	Longitude	Altitude	T	pH	Cl^-	SO_4^{2-}	Na^+	K^+	Ca^{2+}	Mg^{2+}	NO_3^-	F^-	Br^-	NH_4^+	δD	$\delta^{18}O$
Pet5	#2	March 2011	6099157	357050	3331	43.2	1.49	44	3300	82	130	220	140	2.0	5.2	0.06	10.0	−74	−9.5
Pet9	#4	March 2011	6099324	356704	3353	19.1	2.73	200	3000	180	42	330	380	1.0	9.9	0.77	4.9	−80	−9.9
Pet10	#1	March 2011	6098725	357071	3263	7.4	2.91	660	2000	140	34	520	180	1.0	39	1.4	2.6	−80	−10
Pet5	#2	March 2012	6099157	357050	3331	30.6	1.50	92	2800	63	16	180	95	0.81	2.4	0.52			

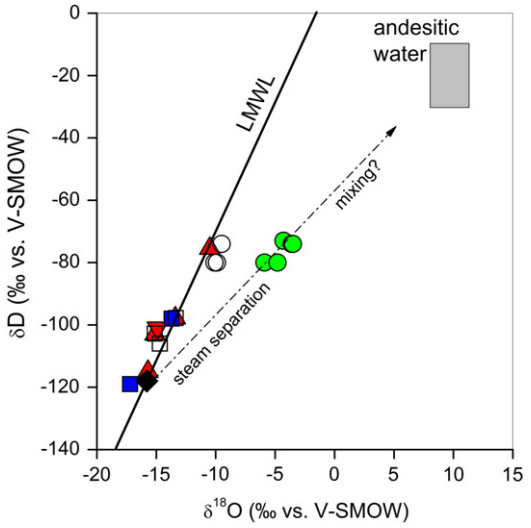

Fig. 3. $\delta D–H_2O$ vs. $\delta^{18}O–H_2O$ diagram of steam from the fluid discharges, bubbling pools, and lake waters from PPAVC. The Andesitic water field (Taran et al., 1989; Giggenbach, 1992), Local Meteoric Water Line (LMWL; Hoke et al. 2013) and isotopic composition of the rainwater collected in this section of the Andes at 4000 m a.s.l. (black diamond) are reported. Green circle: 2011 Peteroa fluid discharge; red up triangle: 2012 Peteroa fluid discharge; blue square 2015 Peteroa fluid discharge; red down triangle: Azufre fluid discharge; white square: water from bubbling pool; white circle: lake water.

Gases from the bubbling pools, which were located at the base of PPAVC, were characterized by the typical composition of peripheral, low-temperature fluid discharges receiving relatively low magmatic fluid contribution, i.e. absence of acidic gases and relatively high concentrations of atmospheric gases (N_2, O_2 and Ar) and CH_4. Accordingly, their $\delta^{13}C–CO_2$ values, more negative than the typical range of gases released from volcanoes in subduction areas (Pineau and Javoy, 1983), suggest a ^{12}C-rich crustal source, whereas their Rc/Ra values showed variable inputs of mantle vs. crustal He. Accordingly, the negative $\delta^{15}N$ value measured in the Cur gas (Table 3) implies N_2 contribution from degradation of fresh organic matter likely occurring at relatively shallow depth. Bubbling gases did not apparently suffer any modification during the study period. On the contrary, dramatic changes affected both the chemical and isotopic characteristics of the Peteroa summit gases.

6.2. Crustal vs. magmatic sources in 2010–2015

The temporal evolution of the isotopic signature of steam from the Peteroa fluid discharges provided one of the strongest evidence of the changes that affected this system from 2010 to 2015. As shown in Fig. 3, the 2011 gas samples from the summit area plot at intermediate position between the local meteoric water line (LMWL; Hoke et al., 2013) and the Andesitic water field (Taran et al., 1989; Giggenbach, 1992) (Fig. 3). The relatively low concentrations of HCl in these samples (Table 1) suggest that a direct contribution of a magmatic brine to the gases appeared to be unlikely, although it cannot be excluded a priori. Hence, the most reliable explanation for these isotopic data is fractionation caused by the separation of steam from an aquifer at T > 200 °C. On the contrary, steam samples collected in 2012 and 2015 had a clear meteoric signature, i.e. similar to that of the waters from the bubbling pools and the crater lakes. An increase of the meteoric water contribution to the 2012 and 2015 fluid discharges, possibly related to ground permeability changes due to the 2010–2011 eruptive activity, may explain both the lack of isotopic fractionation, affecting the steam in 2011, and the decrease of the Xg values show in 2012. The $\delta^{13}C–CO_2$ values (Table 3), which in 2011 approached the value of mantle-related fluids (~ − 5‰ vs. V-PDB; Pineau and Javoy, 1983), in 2012 were significantly more negative (Table 3). Although the $\delta^{13}C–CO_2$ values do not provide an unambiguous parameter to distinguish between mantle and crustal CO_2 (Sherwood Lollar et al., 1997), these changes seem to indicate that in 2012 a significant increase of crustal-type, ^{12}C-rich fluids occurred. The temporal evolution of the Rc/Ra ratios, showing a significant enrichment in ^4He in 2012 and, at a lower extent, in 2014 with respect to the values measured in 2011 and 2015, seems to support this hypothesis. On the contrary, the measured $\delta^{15}N$ values (between 4.27 and 5‰ vs. air.) do not allow to clearly discriminate between crustal and magmatic sources. Such a positive isotopic signature is indeed typical of 1) N_2 produced by thermal decomposition of organic material buried in sedimentary material (Jenden et al., 1988; Fischer et al., 2002; Snyder et al., 2003; Inguaggiato et al., 2004) likely involved in the subduction process, and/or 2) low-grade metamorphism affecting NH_4 fixed in the crystal lattices of K-rich minerals (micas and K-feldspars) of crystalline rocks (e.g., Honma and Itihara, 1981; Mingram and Brauer, 2001).

Summarizing, He and Carbon (in CO_2) isotopic parameters consistently indicate that during the 2010–2011 eruptive activity, the Peteroa summit fluid discharges were dominated by a magmatic component that decreased in 2012 and increased again in 2014–2015. Notwithstanding, variable inputs of magmatic vs. crustal fluid contribution cannot exhaustively explain all the observed changes that affected the chemical and isotopic parameters of the Peteroa gases. According to this hypothesis, the dramatic decrease of the R/Ra and $\delta^{13}C–CO_2$ values measured in 2012 would imply an increase of CO_2 and ^4He from a crustal source. However, an enhanced crustal contribution is not consistent with both the $CO_2/^3He$ decrease and the huge SO_2 increase recorded in 2012. The production of SO_2 from a crustal source, such as pre-existing sulfur deposits, needs a significant increase of temperature that conflicts with the flat temporal patterns of both (i) the most sensitive temperature-dependent parameters (H_2 and CO), and (ii) the outlet temperature and flux of the fumaroles. The 2010–2011 activity stopped before the 2012 sampling, thus the possible influence of these events on sulfur remobilization were to be expected to occur during the eruptive activity, not later. Moreover, sulfur remobilization cannot explain the increases of HCl and HF measured in 2012, as well as the synchronous strong variations of N_2, CH_4 and light hydrocarbons (Table 1).

It is worth noting that the process(es) that caused the compositional changes at the Peteroa summit seems to have affected at a minor extent the Azufre gases, since their compositions were intermediate with respect to that observed at Peteroa in 2012 and 2014–2015 (Table 1). As already mentioned, the chemical and isotopic features of the bubbling gases from the surroundings of PPAVC did not show significant temporal variations.

6.3. Magma degassing model

6.3.1. Preliminary assumptions

A tentative explanation for the appearance of the Cl- and S-rich signature in the 2012 Peteroa gas discharges could be involving a gas contribution from a magma characterized by a very advanced extent of degassing. In fact, a gas phase released from strongly degassed magma is typically enriched in species characterized by high solubility in silicate melt (e.g., Cl and S). Recent works (Paonita et al., 2012, 2013; Caliro et al., 2014) have shown that ratios among inert gases and CO_2 can be used to recognize signatures of magma degassing and quantify the degassing degree, even in fumarolic fields where the contribution from underlying hydrothermal systems is significant. According to the relative solubility of Cl > S > CO_2 > He > N_2 in water, the N_2/He ratios are virtually unaffected by interaction with hydrothermal liquids even in gas phases that have suffered a complete removal of Cl and S (Liotta et al., 2010; Paonita et al., 2012). Moreover, the He/CO_2 and N_2/CO_2 ratios increase by no more than 30–40% when S is still present in the residual gases and Cl has completely been scrubbed (Liotta et al., 2010; Paonita et al., 2012). Hence, although the ratios of these gases were

strongly affected by scrubbing due to the hydrothermal system, they were tentatively used as indicators of magma degassing to model the compositional evolution recorded in 2010–2015 at Peteroa. In Fig. 4a, the 2010–2011 Peteroa samples outline a rough sub-vertical trend from high to low N_2/He ratio (see the black arrow). Given that N_2 solubility in any kind of silicate melt composition is much lower than that of He (Iacono-Marziano et al., 2010), the trend qualitatively suggests a growing extent of magma degassing. The decrease of the N_2/He ratio by magma degassing seems to be paralleled by a slight decrease of N_2/CO_2. In contrast, the Cl- and S-richest gases collected in 2012 from the Peteroa summit displayed very high N_2/CO_2 ratios (Fig. 4a) with respect to those of the 2010–2011 gases, suggesting the occurrence of a process able to increase in time the N_2/CO_2 ratio (see gray arrow in Fig. 4a). As

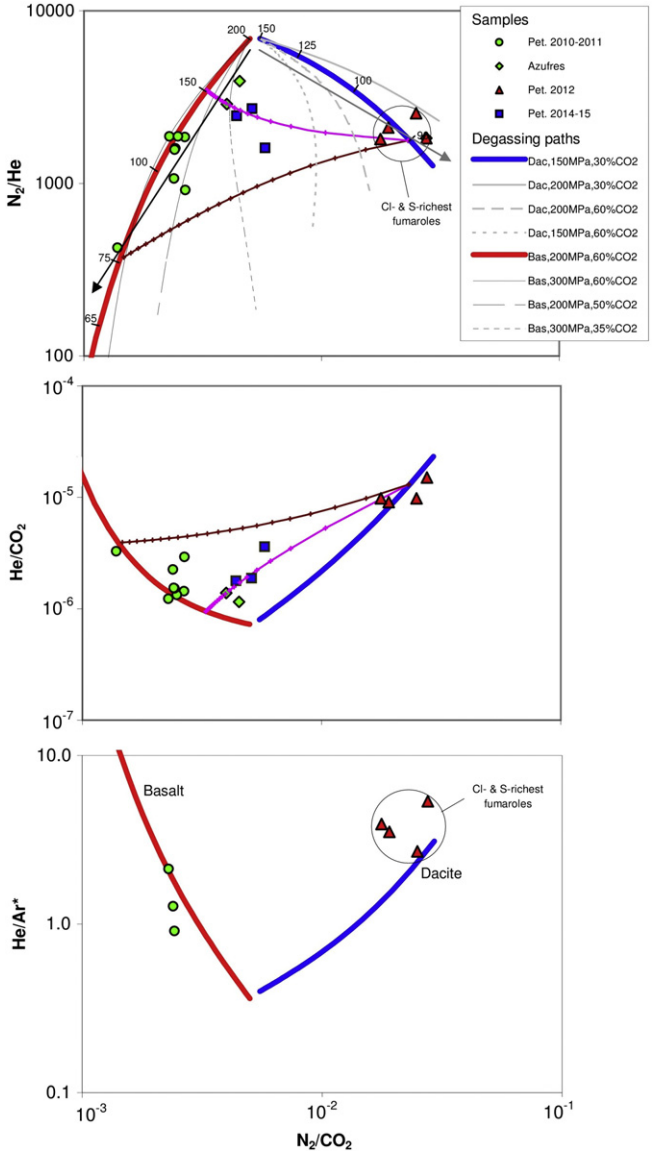

Fig. 4. a) N_2/He, b) He/CO_2 and c) He*/Ar ratios vs. N_2/CO_2 ratios of gases from PPAVC. The N_2 concentrations were corrected for the air contamination based on the measured O_2 contents and the N_2/O_2 atmospheric ratio, whereas Ar* is the air-free Ar content of the samples (see Table 3). The degassing paths are the compositions of vapors released during decompressive degassing of basalt and dacite melts, starting from the initial CO_2 contents and pressures showed in the legend (labels near the curves are degassing pressures in MPa). Initial N_2/He, He/CO_2, He/Ar* and N_2/CO_2 ratios are constrained on the basis of the measured data. The two curves moving from dacite to basalt path refer to mixing of a dacite-exsolved vapor at 90 MPa with basalt-exsolved gases at 160 MPa (magenta) and 76 MPa (brown); the marks on the curves are 5% mixing far each other.

modeled by Caliro et al. (2014), the N_2/CO_2 ratio during magma degassing strongly depends on silicate melt composition, as the ratio decreases during degassing of mafic magmas while it increases for more evolved melts. Therefore, the Cl- and S-rich signature of the 2012 samples was possibly caused by degassing of a magma batch with a more evolved composition than that of 2010–2011. With the aim to quantitatively explore this hypothesis, the isothermal degassing model for H_2O–CO_2–N_2–He–Ar mixtures by Nuccio and Paonita (2001), with the recent upgrades proposed by Caliro et al. (2014), was applied. The model computed the compositional change of the gas phase released from a magma during its progressive decompression, according to the vapor-melt partition coefficients of the involved gases.

Briefly, the adopted solubility values for H_2O–CO_2 mixed vapor and noble gases were from Papale et al. (2006) and from Iacono-Marziano et al. (2010) and Paonita et al. (2012), respectively. Following Caliro et al. (2014), the proposed approach was to:

1) compare the results from the Papale et al. (2006) model with the experimental data by Lesne et al. (2011) and Behrens et al. (2004) for basaltic and dacitic magmas, and properly regulate the FeO/Fe_2O_3 ratio of the model to fit the experimental results; 2) use Ar solubility as a proxy for predicting N_2 solubility in silicate melts; 3) use the experimental relationship of He and Ar solubility versus dissolved H_2O in melt found by Paonita et al. (2000, 2012) in order to compute the effects of H_2O on Henry's constant of the inert gases.

To provide a semi-quantitative interpretation of the acidic gas contents in terms of degassing processes, S was included in the Nuccio and Paonita (2001) model by following the approach of Aiuppa et al. (2004). This requires to deal with S as a minor species and to select a proper fluid-melt partition coefficient (Df-m). The value of Df-m for basalt was the pressure-dependent one (Aiuppa et al., 2004), which resulted to be in agreement with the experimental data by Beermann (2010) for slightly oxidizing conditions (>NNO; see also Fig. 8 in Webster and Botcharnikov, 2011). Based on the review of experimental data by Webster and Botcharnikov (2011), a ratio of Df-m between dacite and basalt of 50 was considered to compute the dacite partition coefficient.

To investigate the effects of silicate melt composition, the spectrum of Peteroa magmas was covered by simulating basalt and dacite degassing (Naranjo and Haller, 2002) at 1150 °C and 1050 °C, respectively. There are no data of volatile contents in melt inclusions able to constrain the pressures of the magmatic reservoirs to be used as starting conditions at Peteroa. Nevertheless, widespread presence of both plagioclase and disequilibrium textures indicates that dacite melts evolved at low pressure, whereas for basalts the increase of Al_2O_3 with decreasing MgO addresses to moderate pressure of differentiation. It is worth noting that the seismic activity closest to the active center of Peteroa was focused within 8 km of depth (see Sect. 3), suggesting pressures lower than 190 MPa (with 2.4 g/cm^3 average density of the lithostatic column). With these constraints, the initial degassing pressures of basalt and dacite were assumed at 200 and 150 MPa, respectively. The initial N_2/He, He/CO_2, He/Ar* and N_2/CO_2 ratios of the magmatic gas phase were considered as parameters to be fit to fumarolic data, since information on the composition of the magmatic vapor at depth (e.g., fluid inclusions data) is not available.

6.3.2. Changes in the magmatic system over time

The compositions of the gas phase from decompressive degassing of basaltic and dacitic magma were computed starting from the initial conditions discussed above. The simulated data are plotted in Fig. 4a,b,c as degassing paths, and compared to the measured fumarolic compositions. It is worth noting that starting from a narrow span of initial ratios for basalt and dacite melts, the divergence of the two degassing paths is able to cover the entire compositional range of the fluid discharges, offering a new context to interpret the temporal evolution of the chemical parameters. Assuming that the initial pressure of magma degassing was 200 MPa, the composition of the 2010–2011 gases is consistent with the

degassing paths for basalt at 75–170 MPa, namely 3 to 6.5 km depth and CO_2 contents in the initial gas phase > 35 mol% (Fig. 4a). On the contrary, the Cl- and S-rich 2012 gases fit with the degassing pathway of a magma with a dacitic composition (Figs. 4a,b,c) at an initial pressure of 150 MPa and a CO_2 content ~30 mol% (Fig. 4a). This value could easily move to 45 mol% assuming an initial pressure of 200 MPa, given that these two parameters cannot be definitely constrained. The 2014–2015 gases plot in between the degassing curves of dacite and basalt, suggesting that in this period the fumaroles were fed by both magma batches degassing at 90 and 150 MPa, respectively (Fig. 4a,b). This may imply that in 2014–2015 the Peteroa magmatic system was slowly restoring the 2010–2011 conditions, as confirmed by the similar Rc/Ra and $\delta^{13}C$–CO_2 values of the 2010–2011 and the 2014–2015 fumaroles, although the latter were still showing the meteoric isotopic signature of steam that characterized the 2012 gases. It is worth noting that the basaltic/dacite degassing pathway of the 2014–2015 Peteroa fluid discharges also includes the 2012 Azufre gases. This suggests that the phenomenon occurred in 2012 was mostly localized at the Peteroa summit, being able to affect Azufre only at limited extent and not modifying the chemistry of bubbling gases at the foothill of the PPAVC (Table 1).

The developed interpretative framework also allowed to model the S (and Cl) variations too. It has to be remarked that these computations are less confident than those of inert gas species, due to the poorly constrained S solubility in the melt. As shown in Fig. 5, two different initial C/S ratios were assigned to basalt and dacite in order to fit the data. The mafic melt would release an early vapor richer in C, which would be compatible with the more primitive origin of this melt. The most remarkable feature is the higher slope of the basalt degassing path with respect to that of dacite (Fig. 5). Starting from an initial N_2/He ratio of 6900 for both basalt and dacite and decreasing it to ~2200, the C/S ratio drops by 15–20 times for the dacite-released vapor, but by less than 2 times for the basalt one. Therefore, at equal N_2/He ratio, the released vapor from dacite, i.e. the 2012 gases, would be ~10 times richer in S than that from basalt feeding the 2010–2011 fluid discharges.

Taking also into account that the initial C/S ratio was lower in dacite than in basalt, a change from a basaltic to dacitic degassing magma batch is able to explain the two-orders-of-magnitude increase of acidic gases in the 2012 gases. As highlighted by Figs. 4a,b,c and 5, the 2014–2015 gases mark transitional conditions between basalt- and dacite-derived vapors. Accordingly, their SO_2 concentrations are much lower than those of the 2012 gases, but slightly higher than in 2010–2011. The occurrence of fluids released from dacite, typically characterized by a more pronounced crustal isotopic signature with respect to those from a parent basalt, also provided a reliable explanation for the puzzling drop of Rc/Ra and $\delta^{13}C$–CO_2 values of the 2012 gases (Rc/Ra = 4.8 and $\delta^{13}C$–$CO_2 = -11.5$). Temporal variations of He and CO_2 concentrations and isotopic values were also measured in fumarolic fluids from Poas volcano (Costa Rica) by Hilton et al. (2010), who interpreted their observation as related to variable inputs of magmatic vs. hydrothermal fluids. However, this explanation cannot be adopted for the 2010–2015 Peteroa gases, since it is not consistent with the measured compositional changes that affected the acidic gases and the hydrocarbons. As already mentioned, the calculated $CO_2/^3He$ ratios, ranging from 1.4 to 8.5×10^{10}, showed a decrease in 2012 (Table 3), apparently indicating an increase of the mantle-related fluid contribution (Sano and Marty, 1995), in contrast with the temporal evolution of both the Rc/Ra and $\delta^{13}C$–CO_2 values. On the contrary, the temporal pattern of the $CO_2/^3He$ ratio is consistent with the decrease of the C/S ratios at equal N_2/He ratios related to a change of the dominant degassing magma batch (Fig. 5).

The model proposed in this study is also consistent with the trace element patterns of the dacitic volcanic products pertaining to PPAVC, which indicates an evolution in shallow crustal reservoirs with a remarkable assimilation of upper crust components (Tormey et al., 1995).

6.4. Gas geothermometry

With the aim to obtain information on temperature and redox conditions of the Peteroa–Azufre magmatic-hydrothermal system and their evolution in time, gas geothermometry in the CO–CO_2–H_2–H_2O system was carried out by considering the following pressure-independent chemical reaction:

$$CO_2 + H_2 \Leftrightarrow CO + H_2O. \quad (2)$$

The dependence on temperature of reaction (2) is given by:

$$\log(CO/CO_2 = 2.49 - 2248/T(K) + R_H) \quad (3)$$

where R_H, i.e. $\log(H_2/H_2O)$, is the most suitable parameter describing redox potentials controlling fluids from volcanic/hydrothermal environments (Giggenbach, 1987). The grid of equilibrium temperatures ranging from 100 to 375 °C in the $\log(X_{H2}/X_{H2O})$ vs. $\log(X_{CO}/X_{CO2})$ diagram (Fig. 6) was constructed by using Eq. (3). We also show equilibrium compositions at R_H values externally fixed in a vapor phase by i) the SO_2–H_2S redox pair (SO_2/H_2S: 1 and 10), typically dominating in fluids from active volcanoes and ii) the redox buffer proposed by D'Amore

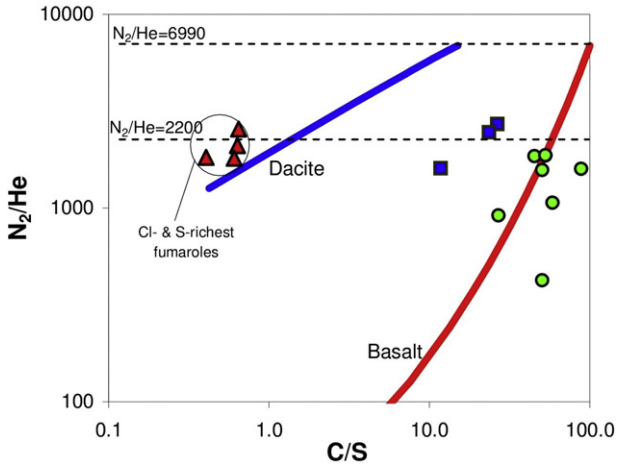

Fig. 5. N_2/He vs. C/S of gases from PPAVC. Degassing paths for basalt and dacite are reported. Initial C/S ratios were constrained on the basis of the measured data. Symbols as in Fig. 4.

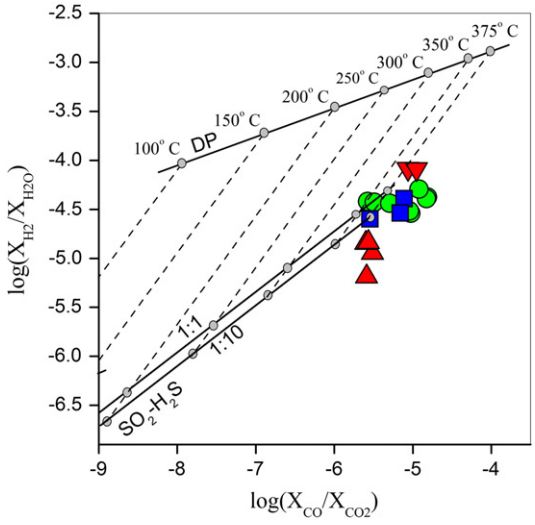

Fig. 6. $\log(X_{H2}/X_{H2O})$ vs. $\log(X_{CO}/X_{CO2})$ diagram for gas samples from Peteroa and Azufre volcanoes. Solid lines refer to equilibria controlled by the DP (D'Amore and Panichi 1980) and the SO_2–H_2S redox buffers (SO_2/H_2S: 1 and 10). Dashed lines are the calculated isotherms from 100 °C to 375 °C for the simultaneous equilibrium of the H_2–H_2O and the CO–CO_2 geothermometers. Symbols as in Fig. 3.

and Panichi (1980) (DP) for hydrothermal systems. All gases approached equilibrium at temperatures ≥350 °C at redox conditions controlled by the SO_2–H_2S buffer. The 2012 Peteroa fluid discharges had relatively low $\log(X_{H2}/X_{H2O})$ values, suggesting more oxidizing conditions, in agreement with their enhanced concentrations of magmatic gases.

Further indications were gathered by considering chemical equilibria of reactions involving hydrocarbons. The Sabatier reaction between CO_2 and CH_4 can be expressed, as follows:

$$CO_2 + 4H_2 \Leftrightarrow CH_4 + 2H_2O. \quad (4)$$

In a vapor phase in equilibrium with boiling pure water, the dependence of the $\log(X_{CO2}/X_{CH4})$ values on temperature and R_H is given by:

$$\log(X_{CH4}/X_{CO2}) = 4R_H + 5181/T + 0.14 \quad (5)$$

The log (X_{H2}/X_{H2O}) vs. $\log(X_{CH4}/X_{CO2})$ diagram (Fig. 7) shows that the CH_4–CO_2 pair was far from the equilibrium conditions suggested by the CO–CO_2–H_2–H_2O system. In fact, at the high temperatures and oxidizing redox conditions indicated by the H_2/H_2O and CO/CO_2 molar ratios (Fig. 6), equilibrated CH_4 should be present in concentrations lower than 4 orders of magnitude with respect to those the measured in the fluid discharges (Fig. 7).

The occurrence of a CH_4-excess would imply CH_4 addition from an "external" source. The ratios between CH_4 and the sum of C_2 and C_3 alkanes, i.e. C_2H_6 and C_3H_8, are from 14 to 212, a range of values consistent with that of thermogenic hydrocarbons (Whiticar, 1999). This suggests that these organic species were added to the uprising magmatic fluids at relatively shallow depth, being produced by degradation of organic material buried in the sedimentary formations surrounding the volcanic system. The relatively slow kinetic of reaction (4) would explain the limited variations of the CH_4/CO_2 ratio (less than 0.5 log-units) in response to the strong compositional changes occurred in 2012. On the contrary, dehydrogenation reactions of the C_2 and C_3 alkene–alkane pairs are considered particularly sensitive to changes of chemical–physical conditions (e.g., Seewald, 1994; Capaccioni and Mangani, 2001; Capaccioni et al., 2004; Taran and Giggenbach, 2003; Tassi et al., 2005). A generic expression for dehydrogenation of alkanes can be expressed, as follows:

$$C_nH_{2n+2} \Leftrightarrow C_nH_{2n} + H_2. \quad (6)$$

Theoretical alkene/alkane molar ratios in the vapor phase can be computed from:

$$\log(X_{C2H4}/X_{C2H6}) + \log(X_{H2}/X_{H2O}) = \log K_1 - \log P_{H2O} \quad (7)$$

and

$$\log(X_{C3H6}/X_{C3H8}) + \log(X_{H2}/X_{H2O}) = \log K_2 - \log P_{H2O} \quad (8)$$

for the C_2 and C_3 alkene-alkane pairs, respectively. The temperature dependence of K_1 and K_2 is given by (Taran and Giggenbach, 2003):

$$\log K1 = 6.82 - 7337/T \quad (9)$$

and

$$\log K_2 = 6.32 - 5676/T(K) - 222490/T^2 \quad (10)$$

where T is in K.

The $\log(X_{C2H4}/X_{C2H6})$ values plotted vs. $\log(X_{H2}/X_{H2O})$ (Fig. 8) confirm that the 2010–2011 and 2014–2015 gases attained chemical equilibrium in a vapor phase at high temperature (>320 °C) and redox conditions consistent with those dictated by the equimolar SO_2–H_2S pair, whereas the 2012 gases are shifted toward more oxidizing conditions ($SO_2/H_2S = 10$). Similar thermodynamic conditions likely controlled the C_3H_6–C_3H_8 pair (Fig. 9). Therefore, chemical reactions governing the C_2 and C_3 alkene–alkane had a similar behavior than those in the CO–CO_2–H_2–H_2O system, supporting the hypothesis that in 2012 an enhanced contribution of oxidizing (SO_2-rich) fluids occurred.

7. Conclusions

The low temperature fluid discharges from the summit of PPAVC are the surficial expression of a dynamic magmatic/hydrothermal system that in 2010–2015 suffered significant modifications. In February 2010 and March 2011, the chemical composition of the discharged fluids had a dominant hydrothermal signature, with relatively low concentrations of gases from magma degassing, notwithstanding the eruptive

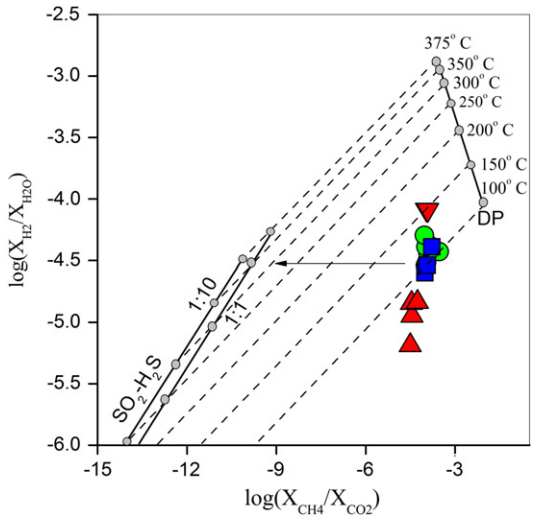

Fig. 7. $\log(X_{H2}/X_{H2O})$ vs. $\log(X_{CH4}/X_{CO2})$ diagram for gas samples from Peteroa and Azufre volcanoes. Solid lines as in Fig. 6. Dashed lines are the calculated isotherms from 100° to 375 °C for the simultaneous equilibrium of the H_2–H_2O and the CH_4–CO_2 geothermometers. Symbols as in Fig. 3.

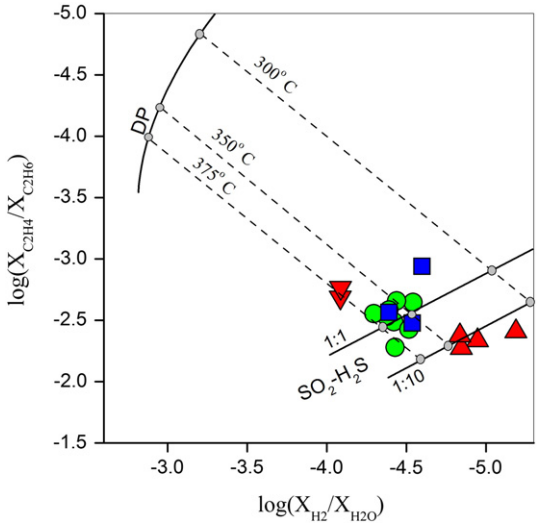

Fig. 8. $\log(X_{H2}/X_{H2O})$ vs. $\log(X_{C2H4}/X_{C2H6})$ diagram for gas samples from Peteroa and Azufre volcanoes. Solid lines as in Fig. 6. Dashed lines are the calculated isotherms from 300 °C to 375 °C for the simultaneous equilibrium of the H_2–H_2O and the C_2H_4–C_2H_6 geothermometers. Symbols as in Fig. 3.

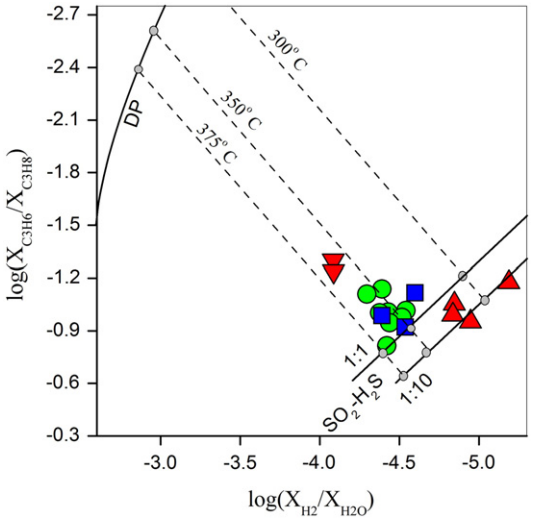

Fig. 9. $Log(X_{H2}/X_{H2O})$ vs. $log(X_{C3H6}/X_{C3H8})$ diagram for gas samples from Peteroa and Azufre volcanoes. Solid lines as in Fig. 6. Dashed lines are the calculated isotherms from 300 °C to 375 °C for the simultaneous equilibrium of the H_2–H_2O and the C_3H_6–C_3H_8 geothermometers. Symbols as in Fig. 3.

events started in January 2010. In March 2012, just few month after the 2010–2011 eruptive activity stopped, the gases from the Peteroa summit showed a huge increase of the acidic gases and a significant decrease of the typical hydrothermal compounds (CH_4 and light hydrocarbons), apparently indicating a pulse of magmatic fluids. On the contrary, the changes in time of the Rc/Ra and $\delta^{13}C$–CO_2 values simulated an input of fluids from a shallow source. This apparent contradiction was tentatively explained hypothesizing a double source of magmatic fluids: (i) a basaltic magma, i.e. the deepest degassing batch that fed the gas discharges in 2010–2011; (ii) a dacitic magma, i.e. a relatively shallow batch likely affected by a significant crustal contamination, whose contribution to the fluid emissions was maximum in 2012. The occurrence of the two magma batches is supported by the basaltic and, secondarily, dacitic volcanic products recognized at PPAVC (Tormey et al., 1995). According to this hypothesis, in 2014–2015, i.e. when the chemical features of the fluid discharges were intermediate respect to those of the two previous periods, both the two magmatic fluid sources were active. Fluids released from the dacitic magma seem to have affected at a minor extent the gases of the Azufre volcano, located few km from the Peteroa summit. Thus, this batch likely have relatively small dimensions, as supported by the tendency shown by the 2014–2015 gases to rapidly restore the 2010–2011 fluid chemistry. It cannot be ruled out that the eruptive activity occurred in 2010–2011 at Peteroa has played a role for the modification of the deep feeding source of the Peteroa fluid discharges. On the other hand, the Maule earthquake occurred in 2010 possibly had a pivotal role in triggering the 2010–2011 eruptions. In fact, large earthquakes are known to be responsible of volcanic events (e.g., Eggert and Walter, 2009), though the driving mechanisms have not clearly understood. The disturbance created by the volcanic events and the related seismic activity could have activated a silent surficial, degassing dacitic magma batch that in 2012 imposed over that of basaltic composition. This scenario provides a reliable explanation for the peculiar compositional changes that affected the Peteroa summit gases in 2010–2015, although such an intriguing hypothesis is expected to be supported by geophysical investigations aimed to locate the two magma sources invoked to construct the proposed degassing model.

Acknowledgments

This study was financed by (1) FONDECYT Iniciación Project No. 11100372 "Role of climate, continental crust and subducted sediments in the degassing style and fluid composition of Andean Volcanoes" and FONDAP No. 15090013 "Centro de Excelencia en Geotermia de los Andes", (2) Universidad de Buenos Aires (UBACyT 20020120300077BA), (3) IDEAN institute (UBA-CONICET) and (4) the Laboratory of Fluid and Rock Geochemistry of the Department of Earth Sciences (Florence, Italy). Many thanks are due to D.R. Hilton, Y. Taran and an anonymous reviewer, whose comments and suggestions have improved an early version of the manuscript.

References

Aguilera, F., Romero, J., Gutierrez, F., Agusto, M., Saltori, O., Benavente, O., Caselli, A., Pizarro, M., 2012. Eruptive activity of Peteroa volcano for Period 2010–2011, Southern Volcanic Zone, Chile. XIII Chilean Geologic Congress 5–9 August, Antofagasta, Chile, pp. 600–602.

Aiuppa, A., Federico, C., Giudice, G., Gurrieri, S., Paonita, A., Valenza, M., 2004. Plume chemistry provides insights into mechanisms of sulfur and halogen degassing in basaltic volcanoes. Earth Planet. Sci. Lett. 222, 469–483.

Barazangi, M., Isacks, B., 1976. Spatial distribution of earthquakes and subduction of the Nazca plate beneath. South Am. Geol. 4, 606–692.

Behrens, H., Ohlhorst, S., Holtz, F., Champenois, M., 2004. CO_2 solubility in dacitic melts equilibrated with H_2O–CO_2 fluids — implications for modelling the solubility of CO_2 in silicic melts. Geochim. Cosmochim. Acta 68, 4687–4703.

Beermann, O., 2010. The Solubility of Sulfur and Chlorine in H_2O-Bearing Dacites of Krakatau and Basalts of Mt. Etna. Ph. D. Thesis, Hannover University, p. 109.

Caliro, S., Chiodini, G., Paonita, A., 2014. Geochemical evidences of magma dynamics at Campi Flegrei (Italy). Geochim. Cosmochim. Acta 132, 1–15.

Cande, S., Leslie, R., 1986. Late Cenozoic tectonics of the southern Chile trench. J. Geophys. Res. 91, 471–496.

Cande, S., Leslie, R., 1987. Interaction between the Chile ridge and Chile trench: geophysical and geothermal evidence. J. Geophys. Res. 92, 495–520.

Capaccioni, B., Mangani, F., 2001. Monitoring of active but quiescent volcanoes using light hydrocarbon distribution in volcanic gases: the results of 4 years of discontinuous monitoring in the Campi Flegrei (Italy). Earth Planet. Sci. Lett. 188, 543–555.

Capaccioni, B., Taran, Y., Tassi, F., Vaselli, O., Mangani, F., Macias, J.L., 2004. Source conditions and degradation processes of light hydrocarbons in volcanic gases: an example from El Chichón volcano (Chiapas State, Mexico). Chem. Geol. 20, 81–96.

Cembrano, J., Lara, L., 2009. The link between volcanism and tectonics in the southern volcanic zone of the Chilean Andes: a review. Tectonophysics 471 (1–2), 96–113.

Coleman, M., Shepherd, T., Rouse, J., Moore, G., 1982. Reduction of water with zinc for hydrogen isotope analysis. Anal. Chem. 54, 993–995.

D'Amore, F., Panichi, C., 1980. Evaluation of deep temperature of hydrothermal systems by a new gas geothermometer. Geochim. Cosmochim. Acta 44, 549–556.

Epstein, S., Mayeda, T., 1953. Variation of the $^{18}O/^{16}O$ ratio in natural waters. Geochim. Cosmochim. Acta 4, 213–224.

Eggert, S., Walter, T.R., 2009. Volcanic activity before and after large tectonic earthquakes: observations and statistical significance. Tectonophysics 471, 14–26.

Evans, W., White, L., Rapp, J., 1998. Geochemistry of some gases in hydrothermal fluids from the southern Juan de Fuca Ridge. J. Geophys. Res. 15, 305–313.

Fischer, T.P., Hilton, D.R., Zimmer, M.M., Shaw, A.S., Sharp, Z.D., Walker, J.A., 2002. Subduction and recycling of nitrogen along the Central American margin. Science 297, 1154–1157.

Giambiagi, L.B., Ramos, V.A., Godoy, E., Alvarez, P.P., Orts, S., 2003. Cenozoic deformation and tectonic style of the Andes between 33° and 34° south latitude. Tectonics 22. http://dx.doi.org/10.1029/2001TC001354.

Giggenbach, W.F., 1987. Redox processes governing the chemistry of fumarolic gas discharges from White Island, New Zealand. Appl. Geochem. 2, 143–161.

Giggenbach, W.F., 1992. Isotopic shifts in waters from geothermal and volcanic systems along margins, and their origin. Earth Planet. Sci. Lett. 113 495–510.

Giggenbach, W.F., 1996. Chemical composition of volcanic gases. In: Scarpa, M., Tilling, R. (Eds.), Monitoring and Mitigation of Volcanic Hazards. Springer, Berlin, pp. 221–256.

González-Ferrán, O., 1995. Volcanes de Chile. Instituto Geográfico Militar. Santiago, Chile, p. 639.

Gutierrez, F., Lemus, M., Parada, M., Benavente, O., Aguilera, F., 2012. Contribution of ground altitude difference to thermal anomaly detection using satellite images: application to volcanic/geothermal complexes in the Andes of Central Chile. J. Volcanol. Geotherm. Res. 237–238, 69–80.

Haller, M., Risso, C., 2011. La erupción del volcán Peteroa (35°15′S, 70°18′O) del 4 de Septiembre de 2010. Rev. Asoc. Geol. Argent. 68, 295–305.

Hauser, A., 1990. Hoja Rancagua, VI Región. 1. Serv. Nac. Geol. Min.

Hauser, A., 1993. Remociones en masa en Chile. 45. Serv. Nac. Geol. Min.

Hildred, W., Moorbath, S., 1988. Crustal contribution to arc magmatism in the Andes of central Chile. Contrib. Mineral. Petrol. 98, 455–489.

Hilton, D.R., Ramirez, C.J., Mora-Amador, R., Fischer, T.P., Füri, E., Barry, P.H., Shaw, A.M., 2010. Monitoring of temporal and spatial variations in fumarole helium and carbon dioxide characteristics at Poàs and Turrialba volcanoes, Costa Rica (2001–2009). Geochem. J. 44, 431–440.

Hoke, G.D., Aranibar, J.N., Viale, M., Araneo, D.C., Llano, C., 2013. Seasonal moisture sources and the isotopic composition of precipitation, rivers, and carbonates across the Andes at 32.5–35.5°S. Geochem. Geophys. Geosys. 14 (4), 962–978.

Honma, H., Itihara, Y., 1981. Distribution of ammonium in minerals of metamorphic and granitic rocks. Geochim. Cosmochim. Acta 13, 225–232.

Iacono-Marziano, G., Paonita, A., Rizzo, A., Scaillet, B., Gaillard, F., 2010. Noble gas solubilities in silicate melts: new experimental results and a comprehensive model of the effects of liquid composition, temperature and pressure. Chem. Geol. 279, 145–157.
Inguaggiato, S., Taran, Y., Grassa, F., Capasso, G., Favara, R., Varley, N., Faber, E., 2004. Nitrogen isotopes in thermal fluids of a forearc region (Jalisco Block, Mexico): evidence for heavy nitrogen from continental crust. Geochem. Geophys. Geosyst. 5, Q12003. http://dx.doi.org/10.1029/2004GC000767.
Jara-Muñoz, J., Melnik, D., Brill, D., Strecker, M.R., 2015. Segmentation of the 2010 Maule Chile earthquake rupture from a joint analysis of uplifted marine terraces and seismic-cycle deformation patterns. Quat. Sci. Rev. 113, 1–22.
Jenden, P.D., Kaplan, I.R., Poreda, R.J., Craig, H., 1988. Origin of nitrogen-rich gases in the California Great Valley: evidence from helium, carbon and nitrogen isotope ratios. Geochim. Cosmochim. Acta 52, 851–861.
Lesne, P., Scaillet, B., Pichavant, M., Beny, J.M., 2011. The carbon dioxide solubility in alkali basalts: an experimental study. Contrib. Mineral. Petrol. 162, 163–168.
Liaudat, D.T., Penas, P., Aloy, G., 2014. Impact of volcanic processes on the cryospheric system of the Peteroa Volcano, Andes of southern Mendoza, Argentina. Geomorphology 208, 74–87.
Liotta, M., Paonita, A., Caracausi, A., Martelli, M., Rizzo, A., Favara, R., 2010. Hydrothermal processes governing the geochemistry of the crater fumaroles at Mount Etna volcano (Italy). Chem. Geol. 278 (1–2), 92–104.
Mamyrin, B., Tolstikhin, I., 1984. Helium isotopes in nature. In: Fyfe, W. (Ed.), Development in Geochemistry. Elsevier, Amsterdam, p. 288.
Mingram, B., Brauer, K., 2001. Ammonium concentration and nitrogen isotope composition in metasedimentary rocks from different tectonometamorphic units of the European Variscan Belt. Geochim. Cosmochim. Acta 65, 273–288.
Montegrossi, G., Tassi, F., Vaselli, O., Buccianti, A., Garofalo, K., 2001. Sulfurspecies in volcanic gases. Anal. Chem. 73, 3709–3715.
Naranjo, J., 2012. Principales etapas evolutivas holocenas del volcán Planchón y su reactivación relacionada al megasismo del 27 de Febrero de 2010. XIII Chilean Geologic Congress 5–9 August, pp. 440–441 Antofagasta, Chile.
Naranjo, J., Haller, M., 2002. Erupciones principalmente explosivas del volcán Planchón, Andes del sur (35°15′S). Rev. Geol. Chile 29, 93–113.
Naranjo, J., Haller, M., Ostera, H., Pesce, A., Sruoga, P., 1999. Geología y Peligros del Complejo Volcánico Planchon–Peteroa, Andes del Sur (35°15′S), Región del Maule, Chile—Provincia de Mendoza, Argentina. 52. Serv. Nac. Geol. Min.
Nelson, S.T., 2000. A simple, practical methodology for routine VSMOW/SLAP normalization of water samples analyzed by continuous flow methods. Rapid Commun. Mass Spectrom. 14, 1044–1046.
Nuccio, P.M., Paonita, A., 2001. Magmatic degassing of multicomponent vapors and assessment of magma depth: application to Vulcano Island (Italy). Earth Planet. Sci. Lett. 193, 467–481.
Ozima, M., Posodek, F.A., 1983. Noble Gas Geochemistry. Cambridge University press, Cambridge.
Paonita, A., Gigli, G., Gozzi, D., Nuccio, P.M., Trigila, R., 2000. Investigation of the He solubility in H_2O–CO_2 bearing silicate liquids at moderate pressure: a new experimental method. Earth Planet. Sci. Lett. 181, 595–604.
Paonita, A., Caracausi, A., Iacono-Marziano, G., Martelli, M., Rizzo, A., 2012. Geochemical evidence for mixing between fluids exsolved at different depths in the magmatic system of Mt Etna (Italy). Geochim. Cosmochim. Acta 84, 380–394.
Paonita, A., Federico, C., Bonfanti, P., Capasso, G., Inguaggiato, S., Italiano, F., Madonia, P., Pecoraino, G., Sortino, F., 2013. The episodic and abrupt geochemical changes at La Fossa fumaroles (Vulcano Island, Italy) and related constraints on the dynamics, structure, and compositions of the magmatic system. Geochim. Cosmochim. Acta 120, 158–178.
Papale, P., Moretti, R., Barbato, D., 2006. The compositional dependence of the saturation surface of $H_2O + CO_2$ fluids in silicate melts. Chem. Geol. 229, 78–95.
Pineau, F., Javoy, M., 1983. Carbon isotopes and concentration in mid-oceanic ridge basalts. Earth Planet. Sci. Lett. 62, 239–257.
Poreda, R.J., Craig, H., 1989. Helium isotope ratios in circum-Pacific volcanic arcs. Nature 338, 473–478.
Pritchard, M.E., Jay, J.A., Aron, F., Henderson, S.T., Lara, L.E., 2013. Subsidence at southern Andes volcanoes induced by the 2010 Maule, Chile earthquake. Nat. Geosci. 6 (8), 632–636.
Ramos, V.A., Cristallini, E., Introcaso, A., 2004. The Andean thrust system latitudinal variations in structural styles and orogenic shortening. In: McClay, K. (Ed.), Thrust Tectonics and Hydrocarbon Systems. AAPG Spec Vol. Memoir 82, pp. 30–50.
Sano, Y., Marty, B., 1995. Origin of carbon in fumarolic gas from island arcs. Chem. Geol. 119, 265–274.
Seewald, J.S., 1994. Evidence for metastable equilibrium between hydrocarbons under hydrothermal conditions. Nature 370, 285–287.
SERNAGEOMIN-OVDAS, 2010a. Actividad volcánica Región del Maule, Grupo volcánico Planchón–Peteroa. Reporte Especial Actividad Volcánica 1.
SERNAGEOMIN-OVDAS, 2010c. Actividad volcánica Región del Maule, Grupo volcánico Planchón–Peteroa. Reporte Especial Actividad Volcánica. 7.
SERNAGEOMIN-OVDAS, 2011a. Actividad volcánica Región del Maule, Grupo volcánico Planchón–Peteroa. Reporte Especial Actividad Volcánica. 15.
SERNAGEOMIN-OVDAS, 2011b. Actividad volcánica Región del Maule, Grupo volcánico Planchón–Peteroa. Reporte Especial Actividad Volcánica. 23.
Sherwood Lollar, B., Ballentine, C.J., O'Nions, R.K., 1997. The fate of mantle-derived carbon in a continental sedimentary basin: integration of C/He relationships and stable isotope signatures. Geochim. Cosmochim. Acta 61 (11), 2295–2307.
Snyder, G., Poreda, R., Fehn, U., Hunt, A., 2003. Sources of nitrogen and methane in Central American geothermal settings: noble gas and 129I evidence for crustal and magmatic volatile components. Geochem. Geophys. Geosys. 4 (1), 9001.
Stern, C., Futa, K., Muehelnbachs, K., Dobbs, F., Muñoz, J., Godoy, E., Charrier, R., 1984. Sr, Nd, Pb and O isotope composition of Late Cenozoicvolcanics, northernmost SVZ (33–34°S). In: Harmon, R., Barriero, B. (Eds.), Andean Magmatism: Chemical and Isotopic Constraints. Shiva Publishing Cheshire, pp. 96–105.
Taran, Y.A., Giggenbach, W.F., 2003. Geochemistry of light hydrocarbons in subduction-related volcanic and hydrothermal fluids. In: Simmons, S.F., Graham, I.J. (Eds.), Volcanic, Geothermal, and Ore-Forming Fluids: Rulers and Witnesses of Processes within the Earth. Soc Econ Geol Spec Issue, Littleton, Colorado, pp. 61–74.
Taran, Y.A., Pokrovsky, B., Doubik, Y.M., 1989. Deuterium and oxygen-18 in fumarolic steam and amphiboles from some Kamchatka volcanoes: "andesitic waters". Dokl. Akad. Nauk SSSR 304, 440–443.
Tassi, F., Vaselli, O., Capaccioni, B., Giolito, C., Duarte, E., Fernandez, E., Minissale, A., Magro, G., 2005. The hydrothermal-volcanic system of Rincon de la Vieja volcano (Costa Rica): a combined (inorganic and organic) geochemical approach to understanding the origin of the fluid discharges and its possible application to volcanic surveillance. J. Volcanol. Geotherm. Res. 148, 315–333.
Tormey, D., Frey, F., López-Escobar, L., 1989. Geologic history of the active Azufre–Planchon–Peteroa volcanic center (35°15'S, southern Andes) with implications for the development of compositional gaps. Rev. Asoc. Geol. Argent. 44, 420–430.
Tormey, D., Frey, F., López, L., 1995. Geochemistry of the active Azufre–Planchón–Peteroa volcanic complex, Chile (35°15′S): evidence for multiple sources and processes in a cordilleran arc magmatic system. J. Petrol. 36, 265–298.
Tormey, D., 2010. Managing the effects of accelerated glacial melting on volcanic collapse and debris flows: Planchon–Peteroa volcano, southern Andes. Glob. Planet. Chang. 74, 82–90.
Varekamp, J.C., Pasternack, G.B., Rowe, G.L., 2000. Volcanic lake systematics II. Chemical constraints. J. Volcanol. Geotherm. Res. 97, 161–179.
Vaselli, O., Tassi, F., Montegrossi, G., Capaccioni, B., Giannini, L., 2006. Sampling and analysis of fumarolic gases. Acta Vulcanol. 18, 65–76.
Webster, J.D., Botcharnikov, R.E., 2011. Distribution of sulfur between melt and fluid in S–O–H–C–Cl–bearing magmatic systems at shallow crustal pressures and temperatures. In: Behrens, J., Webster, H.D. (Eds.), Sulfur in Magmas and Melts: its Importance for Natural and Technical Processes. Rev. Mineral. Geochem. Vol. 73, pp. 247–283.
Whiticar, M.J., 1999. Carbon and hydrogen isotope systematics of bacterial formation and oxidation of methane. Chem. Geol. 161, 291–314.